
Article:
Pitt, K., Tew, J.D., Ahmed, B. et al. (7 more authors) (2024) Spherical agglomeration kinetics: a mechanistic approach. Powder Technology, 445. 120082. ISSN 0032-5910

https://doi.org/10.1016/j.powtec.2024.120082

---

*Corresponding author: Rachel Smith. Email: Rachel.smith@sheffield.ac.uk, Tel: +44 (0)114 2228255

Spherical agglomeration kinetics: A mechanistic approach

Kate Pitt[1], Jonathan D. Tew[1], Bilal Ahmed[1], Cameron Brown[2], Ian Houson[2], Amy L. Robertson[3], Kevin P. Girard[4], Justin L. Quon[5], James D. Litster[1], Rachel M. Smith[1*]

[1] Department of Chemical & Biological Engineering, University of Sheffield, UK

[2] EPSRC CMAC Future Manufacturing Research Hub, University of Strathclyde, Glasgow, UK

[3] AstraZeneca, Chemical Development, Pharmaceutical Technology and Development, Operations, Macclesfield, UK

[4] Pfizer Flexible API Supply, Chemical R&D, Groton, CT, USA

[5] Takeda, 40 Lansdowne Street, Cambridge, MA 02139, USA

Highlights

- Mechanistic approach to understanding spherical agglomeration
- Critical range of bridging liquid to solid ratio identified
- Solid loading and shear influence agglomerate size and porosity
- Model for agglomerate consolidation proposed and validated
- Recommendations for process design given

Graphical Abstract

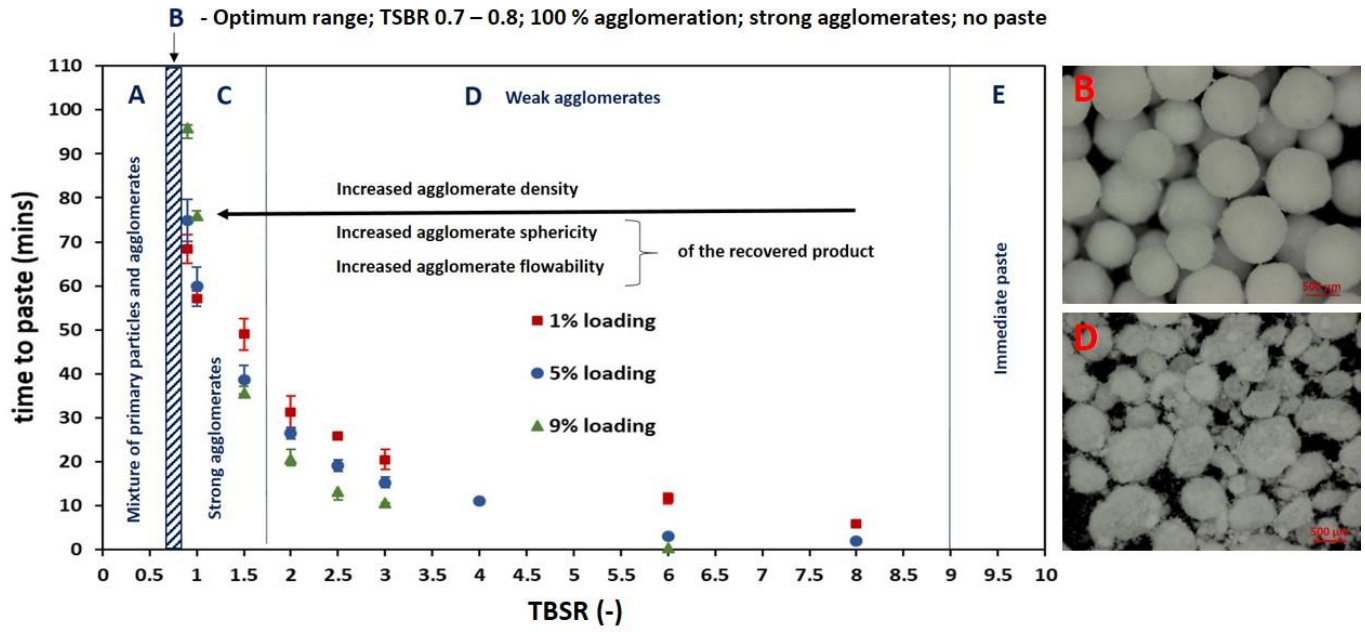

Abstract

Spherical agglomeration, a process of in-suspension particle size enlargement, can substantially improve critical quality attributes of powders. In this work, a paracetamol-heptane-water system is used to investigate the kinetics of spherical agglomeration, demonstrating for the first time the influence of true bridging liquid to solid ratio (*TBSR*) and suspension loading on the evolving size, shape and density of agglomerates. A critical range of *TBSR* is identified where robust agglomerates are formed that are round, moderately dense, and have a controlled size distribution. Immersion nucleation, drop breakage, and agglomerate densification by impact are the controlling rate processes. Increasing mixing intensity reduces agglomerate size, porosity and agglomeration time. Increasing solids loading increases agglomeration time while yielding smaller agglomerates with lower porosity. A first order consolidation model quantitatively predicts the agglomeration kinetics as well as agglomerate properties with increasing *TBSR*, and is a powerful tool for design and scale up.

Keywords

Spherical agglomeration; Spherical crystallisation; Paracetamol; Immersion nucleation; Bridging liquid

1. Introduction

The performance of particulate products is often dictated by the ability to control crucial quality attributes which have a significant influence on powder processing unit operations. In the pharmaceutical industry, crystallization is a routinely applied technique for separation and purification of active pharmaceutical ingredients (API) where attributes of size and shape can impact drug product manufacturability, stability, oral administration route and release kinetics [1]. Undesired aggregation and agglomeration and formation of needle-like crystals are common occurrences in industrial pharmaceutical crystallization, generating downstream processing problems due to broad particle size distribution, poor flow, low bulk density and low compressibility [2-4]. To circumvent these issues, strategies employing additives [5], ultrasound [6] and high shear wet milling [7,8] in addition to the optimization of crystallization parameters have been explored [9]. Whilst improvements can be achieved through external means, in some instances this is only marginal [10].

Spherical agglomeration is an emerging unit operation, capable of performing several particle engineering tasks through the addition of an immiscible or partially miscible bridging liquid into a mother suspension. In this unit operation, existing crystals (typically needle-like) can be manipulated into large and dense spherical particles to improve micromeritic (e.g. size, size distribution, surface area, shape) and functional properties (e.g. strength, flowability, reactivity, solubility and dissolution characteristics) [11]. The early use within the natural resources industry for coal [12], graphite [13] and sand [14] presents an opportunity to engineer APIs to 'tailor-made' properties. Spherical agglomeration can either be performed by simultaneous precipitation and agglomeration or by agglomeration in suspension (post-crystallisation) [11]. However, the technique is still within its infancy stage of research and development as a modern manufacturing technique, and requires further research and development to fulfill its potential within the pharmaceutical industry, particularly for direct compression opportunities [15].

Progress on applying the spherical agglomeration technique has been made on several pharmaceutical compounds through experimental evaluation with an emphasis on the preparation of agglomerates and impact of process parameters (agitation rate, binder to solid ratio etc.) [16-22]. Similarly, population balance models have also been developed to describe the agglomeration mechanism, primarily during the growth-period through agglomerate-agglomerate collisions, crystal-crystal collisions and coalescence of agglomerate nuclei [23-27]. More recently, a population balance model was developed by Ahmed et al. [28] where all the key rate processes to predict agglomerate properties were considered. Reported studies have outlined parallel mechanisms with wet granulation, namely wetting and nucleation, growth and consolidation, attrition and breakage. However, there remains a need to further understand, predict and control these mechanisms for the formation of spherical agglomerates with preferential characteristics [11, 29]. However, there are few careful studies of the *kinetics* of the spherical agglomeration process to support development and validation of these models. There has only been one study in the literature that has reported changes in agglomerate properties (size, porosity, strength) as a function of agglomeration time [22,26]. Thus, a rigorous approach to process design and scale up is not available.

Of critical importance to the agglomeration in suspension method is the initial wetting and nucleation stage which is controlled by both the bridging liquid properties and the addition method [30, 31]. Depending on the relative size ratio between the bridging liquid droplet size and primary crystals, an immersion or distribution mechanism occurs [11].

Here, preference should be given to the immersion route as particles are observed to be more spherical and denser [32]. Recently, two new mathematical models were introduced to predict the kinetics of wetting and subsequent formation of agglomerate nuclei during the immersion method [33]. The identified mechanism for the agglomerate nucleus formation consisted of: initial impact of particles with a single bridging liquid droplet; coverage and initial shell formation composed of particles; expansion of the shell in a growing nucleus; complete filling by crystals inside the bridging liquid droplets. From this work, an *agglomeration nucleation number* was introduced to demarcate the boundary of three different rate limited regimes: *immersion rate; collision rate and; intermediate.* [33].

To enable the routine use of spherical agglomeration for a given pharmaceutical compound, a key controlling parameter is the *bridging liquid to solid ratio (BSR*) [34], which is defined as:

$$BSR = \frac{V_z}{V_s} \tag{1}$$

where V_z is the volume of liquid binder added and V_s is the volume of the solid in the system. Under a given material system of interest, there exists a critical *BSR* range which to date has typically been found empirically. Below this range, looser agglomerates form due to an insufficient amount of bridging liquid, whereas above this range, a paste-like product from excess bridging liquid availability occurs [35]. Identifying and operating within the critical range to produce strong and stable agglomerates for further processing is essential. In pharmaceutical systems, partial miscibility between the solvent/anti-solvent continuous phase and the dispersed bridging liquid phase can reduce the true amount of dispersed phase available for agglomeration. For this reason, the critical *BSR* is very system dependent [11]. Tew et al. [34] defined the true bridging liquid to solid ratio (*TBSR*), based on the actual amount of bridging liquid rich phase available:

$$TBSR = \frac{V_D}{V_S} = \frac{\frac{M_D}{\rho_D}}{\frac{M_S}{\rho_S}} \tag{2}$$

where V_D is the volume of the bridging liquid-rich phase, $V_S$is the volume of solid, M_D is the mass fraction of the bridging liquid-rich phase, ρ_D is the true density of the bridging liquid rich phase, M_S is the mass of solid in the system and ρ_S is the true density of the solid. If the ternary phase diagram for the solvent/antisolvent/dispersed phase is known, it is straightforward to calculate *TBSR* from *BSR*. The critical value of *TBSR* is a more robust and system

independent parameter for design and scale up. TBSR can be calculated relatively easily for a given *BSR* if the solvent-antisolvent-binder phase diagram is known.

Kinetic understanding through careful selection and varying of process parameters within this range is limited in the literature, but is essential to the development of the spherical agglomeration process. In this paper, we present a mechanistic approach for describing the spherical agglomeration process via immersion nucleation using an agglomeration in suspension technique for the spherical agglomeration of paracetamol. The approach is developed through careful study of agglomeration kinetics and the time evolution of agglomerate size, size distribution, density and shape. A model for agglomerate consolidation due to impacts is proposed and tested against these results.

2. Materials and Methods

2.1 Materials

An agglomeration system of paracetamol crystals suspended in heptane was used. Water, saturated with paracetamol, was used as the bridging liquid. This system has the advantage that paracetamol is insoluble in heptane, and water and heptane are immiscible. Therefore, for this system, the *BSR* is equal to the true *BSR* (*TBSR*) [34]. Micronised paracetamol with a d_{50} of 21 μm (Fig. 1) was supplied by the University of Strathclyde. Heptane (99 %) was purchased from Sigma-Aldrich, UK. Distilled water was used throughout. For some experiments, acid red dye (Sigma-Aldrich, UK) was dissolved in the bridging liquid for visual identification in the system.

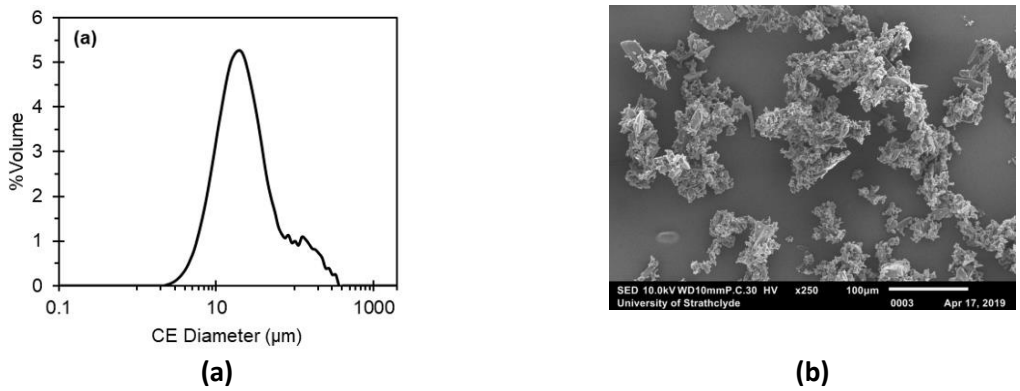

(a) **(b)**

Fig. 1. Micronised paracetamol starting material (a) particle size distribution measured using Malvern Morphologi G3 (b) SEM image.

2.2. Methods

Experimental

All experiments were carried out at room temperature (21 °C). The experimental apparatus consisted of a covered batch stirred tank (glass vessel; diameter = 65 mm, height = 75 mm) and a three bladed pitched impeller (diameter = 40 mm, pitch angle = 30 °). The paracetamol particles were suspended in heptane at various solid loadings (50 g total mass). The bridging liquid was added directly into the stirred suspension using an autopipette (addition time of approximately 1 sec).

For this system, the continuous and dispersed phases are completely immiscible so that *TBSR* = *BSR*. The *TBSR* (by volume) was varied between 0.2 – 8 by varying the amount of bridging liquid added. Three different solid loadings were studied; 1 %wt/wt, 5 %wt/wt and 9 %wt/wt. In all these cases, the impeller speed was 500 rpm. Additionally, at a 5 %wt/wt loading, the impeller speed was varied from 300 rpm – 700 rpm to study the effect of mixing intensity on the agglomeration process. Images of the agglomerates, sampled from the suspension during the process and the recovered end product, were captured using a Lumenera Infinity 3 Camera (Lumenera Corporation, Canada) fitted with a Navitar 12X zoom lens (Image Optics, UK) and a LGT.19.MF2D LED dome diffuser lamp (Honyu, China). Fig. 2 shows images of agglomerate formation during a typical agglomeration process using dyed bridging liquid, confirming immersion nucleation taking place. Bridging liquid droplets can be clearly identified at early times, with primary particles immersing into the droplets as time proceeds, mirrored with a decrease in the number of primary particles in suspension. Eventually dense, spherical agglomerates are produced.

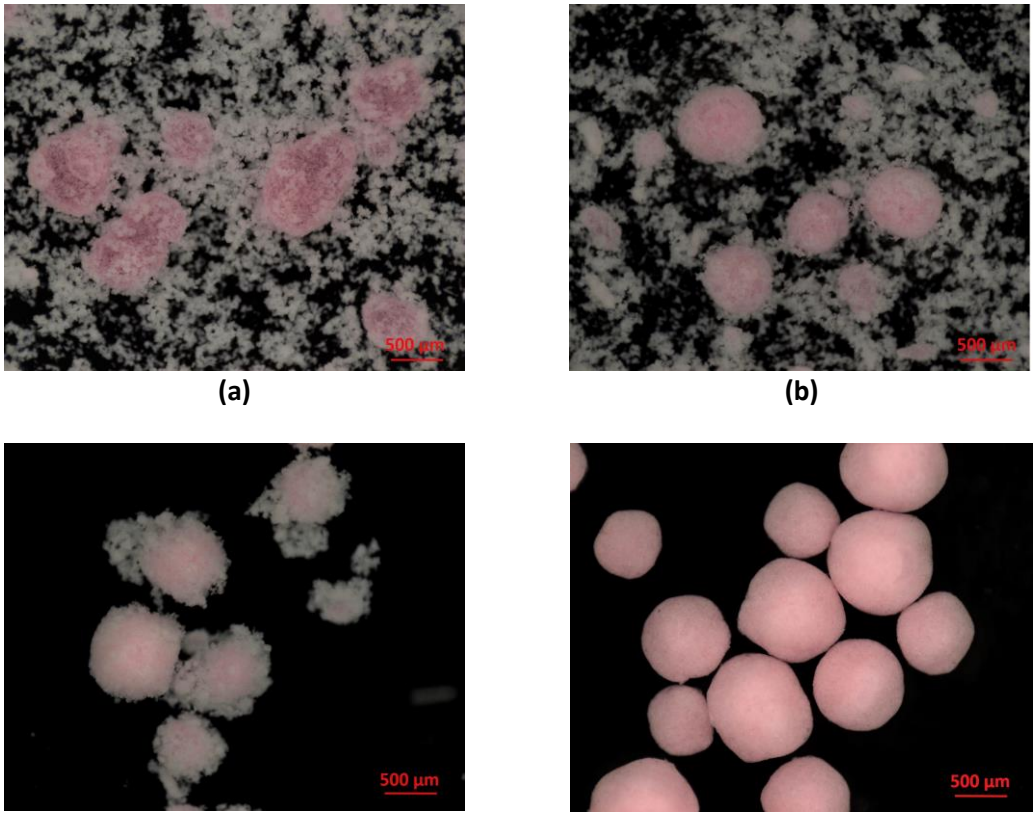

Fig. 2. Typical agglomeration process: agglomerates after (a) 20 mins (b) 50 mins (c) 70 mins (d) 90 mins. Solid loading = 5 %wt/wt, *TBSR* = 0.75, 500 rpm.

Agglomerate characterisation

Agglomerate size and porosity of the end product agglomerates were measured for each of the different operating conditions. At a certain condition (5 %wt/wt solid loading, agitation rate of 500 rpm and a *TBSR* of 0.75) the changes in agglomerate properties (percentage agglomeration, agglomerate porosity, size and sphericity) were measured as a function of agglomeration time.

Experiments to produce agglomerates for size and shape analysis were carried out in either duplicate or triplicate. Image analysis (Pixelink µScope software) was used for agglomerate size and shape measurements. The number of agglomerates measured typically ranged from 500 – 750 per sample, and the agglomerate size was taken as the longest physical dimension. The aspect ratio of the agglomerates was used to characterize shape. Aspect ratio was defined as the shortest physical dimension (d_1) divided by the longest physical dimension (d_2).

Experiments to produce agglomerates to determine porosity measurements were carried out in triplicate. Dry, individual, spherical agglomerates were weighed using a microbalance (Mettler Toledo, UMT2) and the volume of the same agglomerates was determined by measuring the average particle diameter, i.e. $(d_1 + d_2) / 2$, using image analysis. Individual agglomerate density was calculated from the agglomerate mass and volume. A minimum of ten agglomerates were measured for each condition and the mean density calculated. The porosity of the agglomerates (ϕ) can then be calculated from agglomerate density (ρ_{agg}) and the true density (ρ_t) of paracetamol (1.27 mg/mm^3), according to:

$$\phi = 1 - (\rho_{agg} / \rho_t) \quad (3)$$

Experiments were also conducted to determine the extent of agglomeration as a function of time. After a predetermined time, the experiment was stopped and the entire suspension poured into a sieve (212 μm mesh, Retsch) positioned above a Buchner filter (2.7 μm pore size) and washed with a small amount of heptane. The spherical agglomerates were collected in the sieve and the un-agglomerated primary particles resided on the filter paper positioned below. The sieve and filter paper were dried overnight and weighed to determine the percentage agglomeration by mass. It was assumed that all the spherical agglomerates are of a size of above 212 μm. From qualitative observation this appears to be a reasonable assumption, as very few spherical agglomerates below this size were identified using image capture and analysis. Experiments to produce agglomerates for determination of percentage agglomeration were carried out in triplicate.

3. Results

3.1. Agglomeration behaviour and the impact of true bridging liquid to solid ratio (*TBSR*)

Fig. 3 shows a summary plot of the effect of *TBSR* at a solid loading of 5 % and an impeller speed of 500 rpm. Note that for this model system, heptane and water are completely immiscible so that *TBSR* = *BSR*. We use *TBSR* for reporting as it is more system independent. The effect of *TBSR* in terms of the product properties and the time taken for paste formation can be divided into five regions. In *Region A*, there is not enough bridging liquid available to completely agglomerate the primary particles. This results in a mixture of primary particle flocs and dense spherical agglomerates.

The ratio of these products remains the same after a long agglomeration time, implying that all the bridging liquid has been exhausted and no further agglomeration can occur. An example of this behaviour is given in Fig. 4a. The transition from *Region A* to *Region B* is where primary particles are no longer observed. In *Region B* (*TBSR* = 0.7 – 0.8), complete agglomeration occurs, and is termed the optimum *TBSR* range. The agglomerates are dense and spherical (Fig. 4b). Once all solid has been incorporated, there is little to no free bridging liquid available. This absence of free bridging liquid is a barrier to agglomerate coalescence. The product remains stable over long periods of agitation without paste formation, allowing simple recovery of the agglomerates via filtration (Fig. 4c). These agglomerates are relatively strong, as they remain intact during filtration and drying and qualitatively demonstrate excellent flow characteristics. The transition to *Region C* is when coalescence and paste formation occurs within the timescale of the experiment (120 min). In *Region C*, complete agglomeration occurs and the agglomerates are dense and spherical. However, shortly after full agglomeration has occurred, agglomerates start to coalesce, and a paste is formed with continued mixing. Paste formation was observed at times ranging from 38 to 75 min. This is due to an excess of bridging liquid in the system once all the primary particles have been immersed into the droplets. The time for paste formation decreases with increasing *TBSR*. It is possible to collect the agglomerates just before coalescence/paste formation via filtration. The agglomerates survive filtration and agglomeration, and at relatively low *TBSR* (*i.e.* 2) the agglomerates appear dense and highly spherical, similar to those produced in the optimum TBSR range (Fig. 4d). As *TBSR* increases within this region, the agglomerates are weaker, not as spherical, and some breakage is observed during the filtration process (Fig. 4e). The transition to *Region D* is where agglomerates are too weak to survive filtration. In *Region D*, although complete agglomeration occurs, the time for paste formation decreases as the *TBSR* is increased. At higher *TBSR*, the agglomeration process is much quicker and once full agglomeration has been achieved, the excess bridging liquid initiates rapid paste formation. Agglomerates in suspension just prior to paste formation are less dense and less spherical compared to those formed in the lower *TBSR* regions (Fig. 4f). The agglomerate density decreases as the *TBSR* is increased. These agglomerates do not survive filtration. They are weak and collapse during the filtration process (Fig. 4g). The transition to *Region E* is when there is such a large excess of bridging liquid that a paste is formed almost immediately (Fig. 4h).

Region B is the optimum operation range. Operation in *Region C* is also possible provided the agglomeration time is less than time to paste formation. Operation in *Regions A, D* and *F* will not give a suitable product.

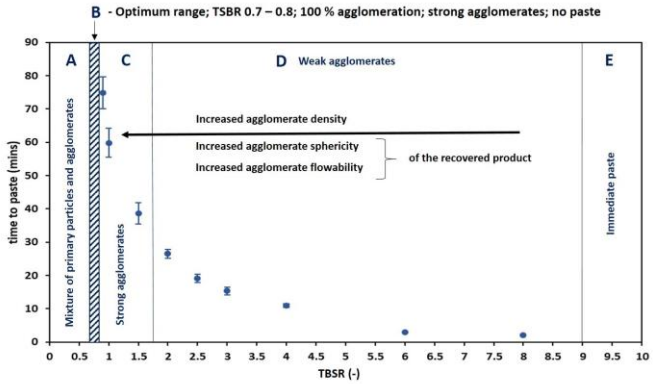

Fig 3. Effect of true bridging liquid to solid ratio (*TBSR*) at a solid loading of 5 % and impeller speed of 500 rpm. Error bars represent the standard error of three experiments.

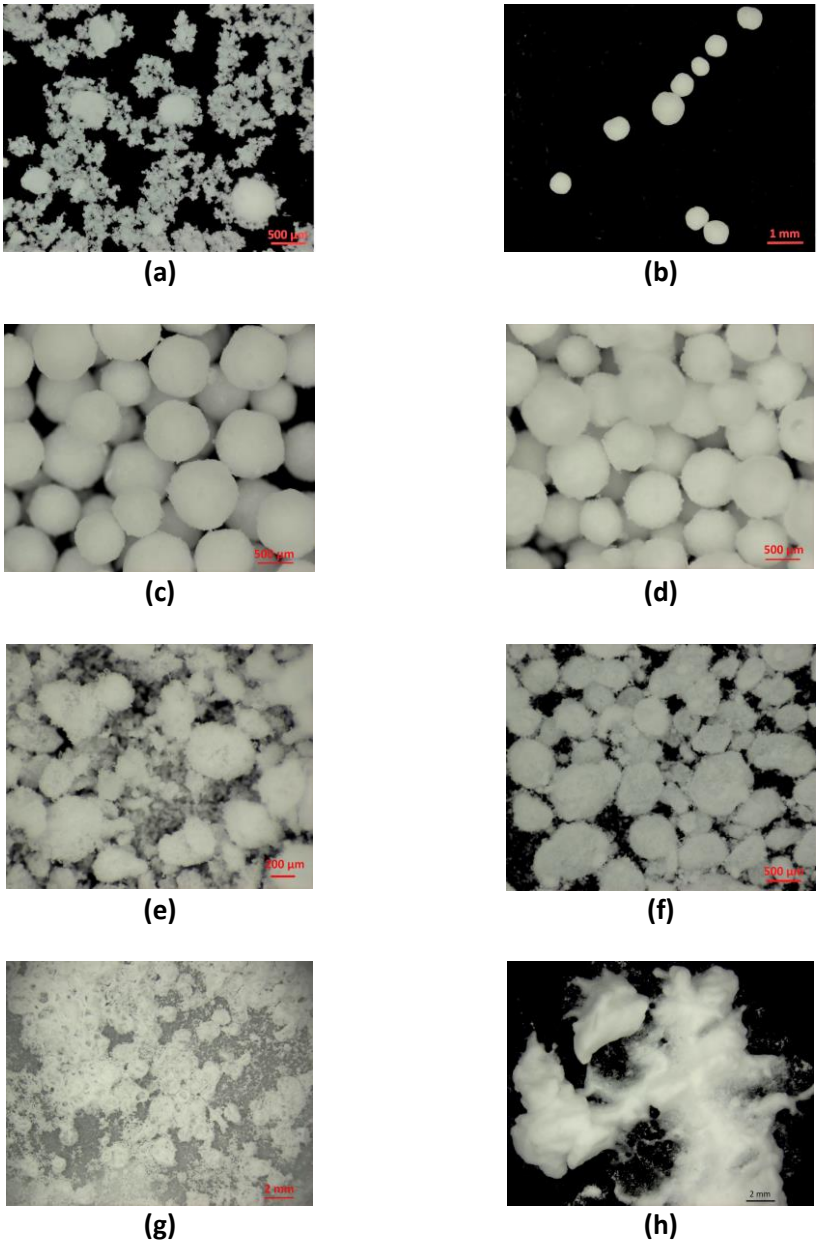

Fig 4. Effect of *TBSR* at a solid loading of 5 %wt and impeller speed of 500 rpm. End product images at (a) *TBSR* = 0.5 (sampled from suspension); (b) *TBSR* = 0.8 (sampled from suspension); (c) *TBSR* = 0.8 (filtered product); (d) *TBSR* = 0.9 (filtered product); (e) *TBSR* = 1.5 (filtered product); (f) *TBSR* = 3 (sampled from suspension); (g) *TBSR* = 3 (filtered product); (h) *TBSR* = 10; paste formation.

3.2 Agglomeration kinetics at optimum TBSR (*Region B*)

Studies to investigate the change in agglomerate properties during the agglomeration process were also carried out. These experiments were conducted in the optimum range (*TBSR* = 0.75), at a solid loading of 5 %wt/wt and impeller speed of 500 rpm. Fig. 5 shows images of the agglomerates as a function of time. The images clearly show that the percentage agglomeration increases with time, as well as the agglomerate density (i.e. the amount of primary particles immersed into the droplets). Fig. 6 shows the percentage agglomerated at each time point. After 96 min, there is nearly 100 % agglomerate formation with very few primary particles left in suspension. Fig. 7 shows agglomerate density (solids concentration) also increases with time, up until 103 min, at which point complete agglomeration was achieved. There is a close coupling between the kinetics of agglomerate density and percentage agglomerated. Fig. 8 shows the agglomerate size and shape data combined in one plot, with three distinct stages. The three stages are demarcated by observation of the agglomerates in Fig. 5, where distinct differences in agglomerate structure are evident. In *Stage I*, immersion nucleation occurs and large, low density agglomerates are initially formed (Fig. 5a and b). These are weak and break up under agitation. A sharp decrease in agglomerate size is accompanied by an increase in agglomerate sphericity. The transition to *Stage II* is where no further agglomerate size reduction occurs. In *Stage II*, further consolidation and capture of primary particles occurs, however there is no change in agglomerate size. At this point, the agglomerates become much denser/stronger than observed in *Stage I*. Although aspect ratio still increases for a time in this region, the agglomerate size remains roughly constant (Fig. 5c-f). This is likely due to both growth and breakage rate processes occurring simultaneously. Smaller breakage fragments are evident in the system as the time approaches 80 min (Fig. 5f). The transition to *Stage III* is when no primary particles remain. However, in *Stage III* some changes to the agglomerate properties were still observed. The dense agglomerates combine/coalesce with the smaller broken agglomerate fragments. This results in an initial decrease in sphericity and increase in agglomerate size as the fragments adhere onto the agglomerate surfaces (Fig. 5g). The amount of broken fragments decreases with increasing agglomeration time in this region until no fragments remain. With continued agglomerate-agglomerate collisions, highly spherical agglomerates are eventually produced (Fig. 5h).

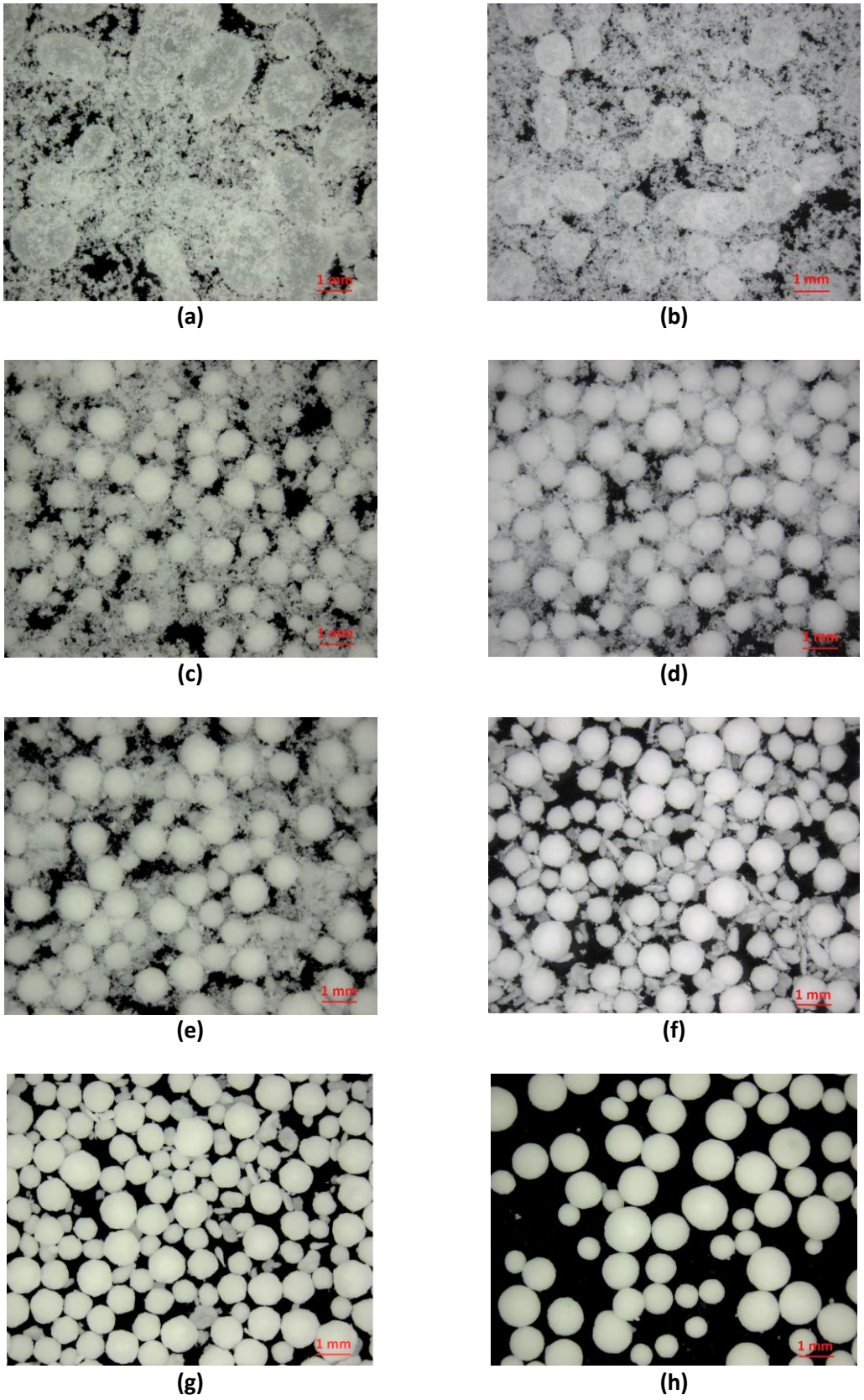

Fig. 5. Images of agglomerates as a function of time: (a) 1 min, (b) 10 min, (c) 30 min, (d) 40 min, (e) 60 min, (f) 80 min, (g) 100 min, (h) 120 min. *TBSR* = 0.75; 5 %wt/wt solid loading; impeller speed = 500 rpm.

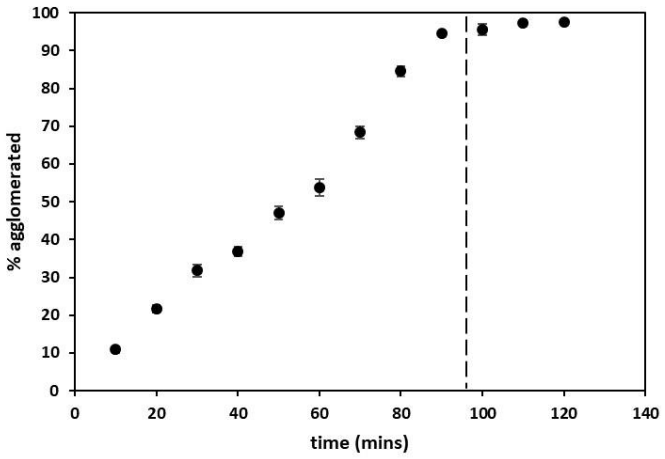

Fig. 6. Percentage agglomeration for each time point. Time for agglomeration (t_{agg}) = 96 min. Error bars represent the standard error of three measurements for each time point.

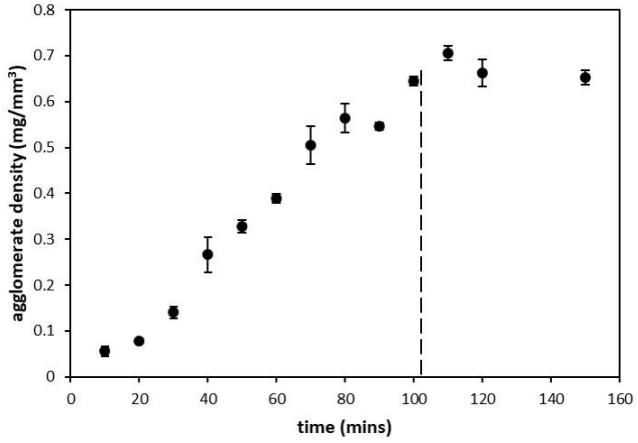

Fig. 7. Density values for each time point. Time to achieve maximum density (t_d) = 103 min. Error bars represent the standard error of three experiments.

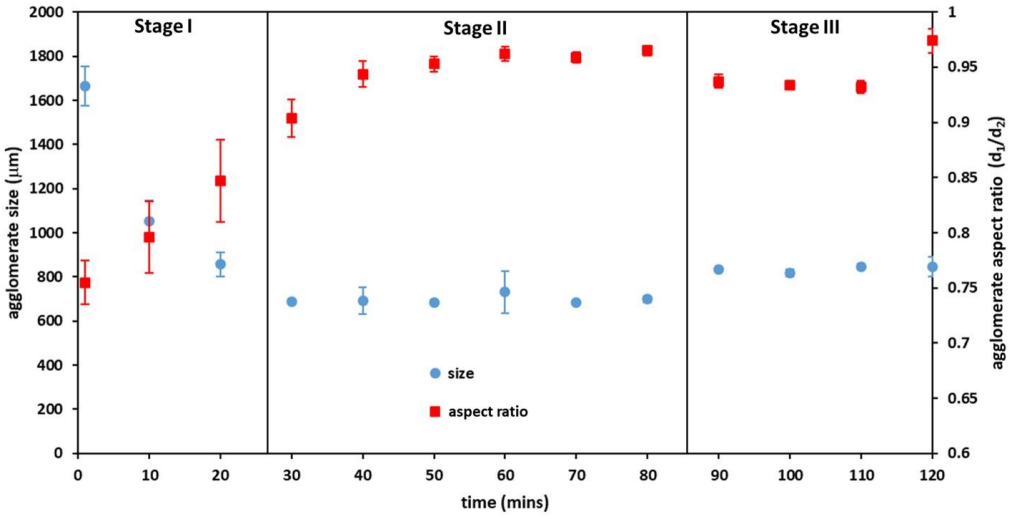

Fig. 8. Agglomerate size and aspect ratio as a function of time. Error bars represent the standard deviation of a minimum of two experiments.

3.3. Effect of agitation rate

The effect of mixing intensity on agglomerate properties in the optimum *TBSR* range was studied by varying the impeller speed. The solid loading and TBSR were kept constant at 5 %wt/wt and 0.75 respectively. Fig. 9a shows the effect of impeller speed on the time to achieve full agglomeration. It is clear that the process is faster at higher agitation rate. The final agglomerate size decreases considerably with an increase in impeller speed (Fig. 9c), accompanied with a narrowing of the size distribution (Fig. 9d). This is mainly due to the higher agitation rate resulting in a smaller initial droplet size due to droplet breakage, leading to smaller agglomerates via immersion nucleation in *Stage I* [33]. A decrease in agglomerate size with increasing agitation rate has been reported by several authors [e.g. 22,36-38] and has previously been attributed to agglomerate breakage. However, this does not appear to be the case here. A higher agitation rate also induces agglomerate compaction due to increased intensity of agglomerate-equipment collisions, and there is a clear decrease in agglomerate porosity with increasing impeller speed (Fig. 9b). This decrease in porosity with increasing agitation rate has also been noted by Blandin et al. [22] for the spherical agglomeration of salicylic acid.

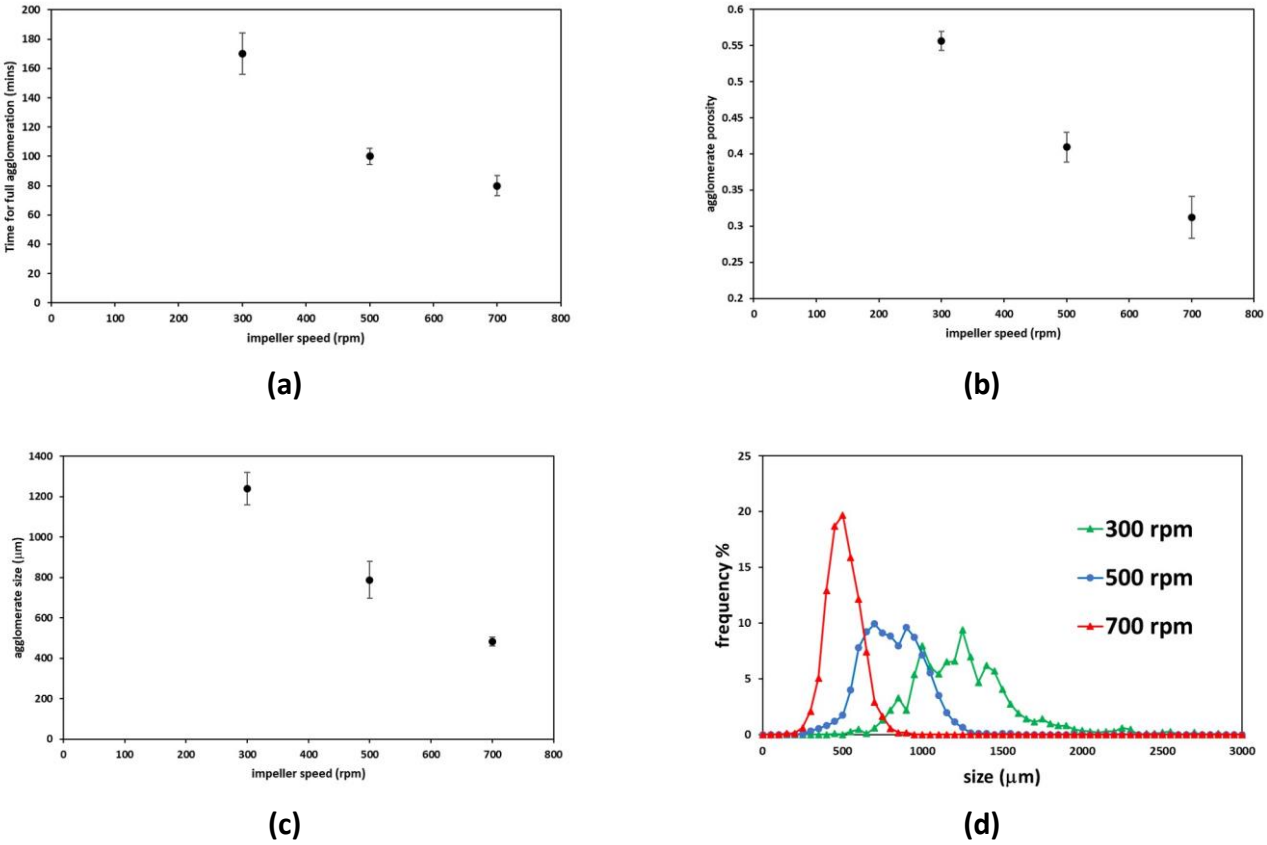

Fig. 9. Effect of impeller speed on agglomerate properties: (a) time for complete agglomeration, (b) porosity, (c) size, (d) size distribution. *TBSR* = 0.75 and solid loading of 5 % wt/wt. Error bars represent the standard error of three experiments.

3.4. Effect of solid loading

Fig. 10 shows the effect of *TBSR* at different solid loadings. The optimum *TBSR* range is demonstrated to be independent of solid loading. The time to paste kinetics and product properties show similar trends with increasing *TBSR* for varying solid loadings. However, the time to paste does show some small dependency on solid loading. At relatively high *TBSR* (in *Region D*), the time to paste is quicker with higher solid loading. As *TBSR* decreases into *Region C*, this effect of a faster time to paste for higher loadings is no longer evident. Indeed, as the *TBSR* is decreased further towards the optimum range, paste formation becomes slower for higher loadings indicating a slower agglomeration process.

Fig. 11a shows the time for full agglomeration for the three different solid loadings for an optimum *TBSR* of 0.75. It is clear that the agglomeration process is much slower for the higher solid loadings for all *TBSRs* in this *Region B*. For example, at *TBSR* = 0.75 and 500 rpm, agglomeration time is increased approximately 3.5 times from 90 min to 330 min (Fig. 11a). These results suggest that for this material system at *TBSR* values lower than 1, agglomerate formation is limited by the volume of the bridging liquid available. As a result, it takes longer for all solid material to be incorporated into the agglomerates formed. Conversely, above a value of 1, the process is not limited by this phenomenon. The bridging liquid is in excess, indicating particles are rapidly wetted and agglomerate growth begins almost instantaneously. This quick depletion of available solid results in agglomerate coalescence and the onset of paste formation.

There is also a decrease in agglomerate size as solids loading increases (Fig. 11c) and a significant narrowing of the size distribution from 1 % loading to 5 % loading (Fig. 11d). Fig. 11b shows that there is also a clear decrease in agglomerate porosity as the solid loading is increased. This coupling between agglomerate size and density is similar to that caused by increased impeller speed. These porosity measurements are in agreement with works by Katta and Rasmuson [36] and Blandin et al. [22] who both reported a decrease in agglomerate porosity with increasing solid loading for benzoic acid and salicylic acid respectively. However, the trends in agglomerate size with solid loading are in contrast to both these works, where an increase in agglomerate size was observed with increased solid loading.

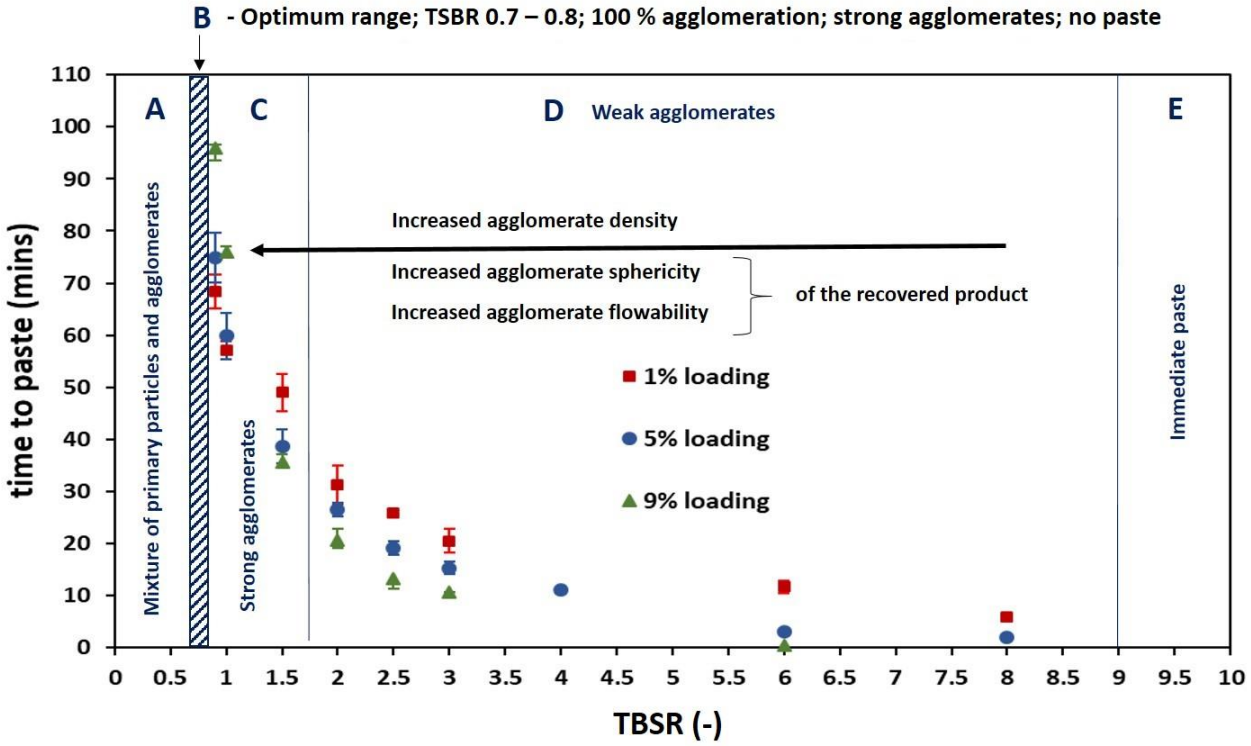

Fig. 10. Effect of true bridging liquid to solid ratio (*TBSR*) at different solid loadings and an impeller speed of 500 rpm. Error bars represent the standard error of three experiments.

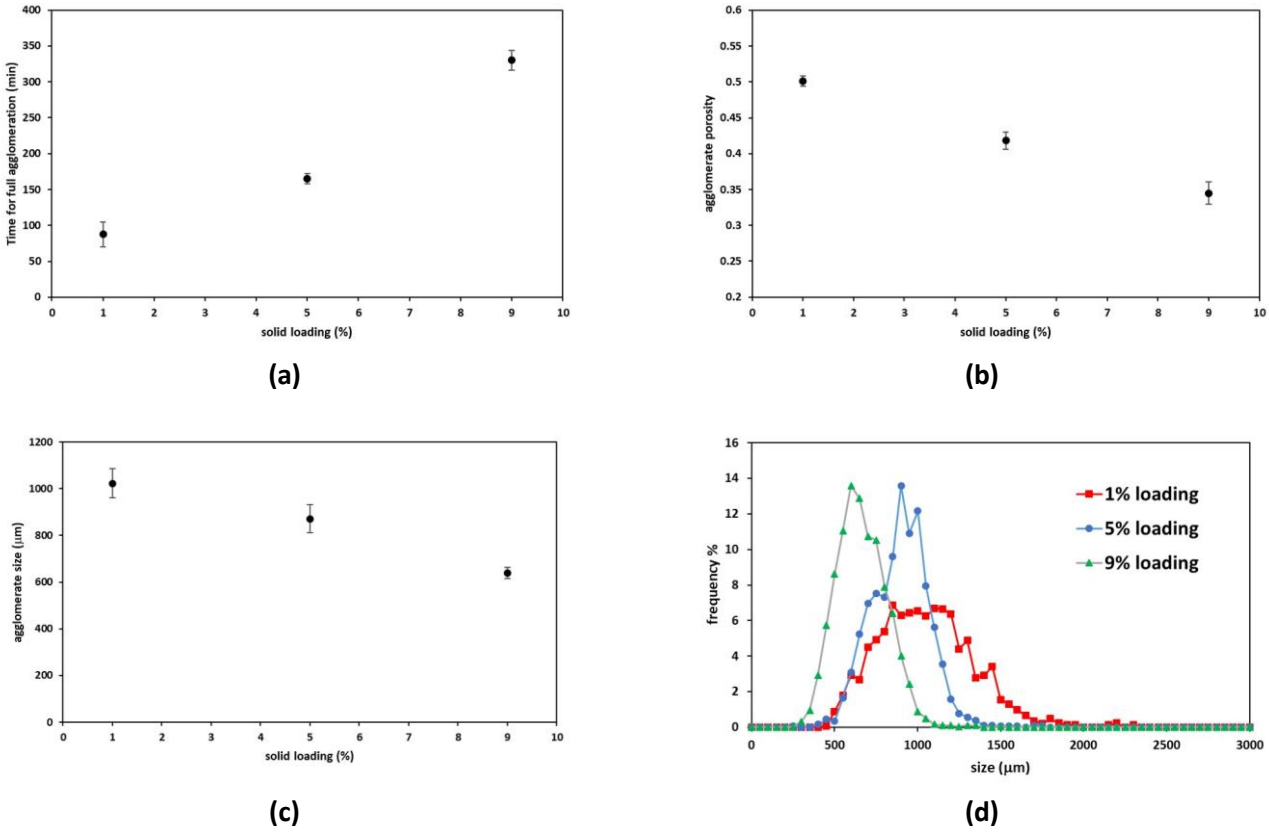

Fig. 11. Effect of solid loading on agglomerate properties: (a) time for complete agglomeration, (b) porosity, (c) size, (d) size distribution. *TBSR* = 0.75 and impeller speed of 500 rpm. Error bars represent the standard error of three experiments.

4. A model for agglomerate consolidation and growth

This study clearly shows there is a narrow range of *TBSR* (*Region B and C*) in which robust agglomerates are formed that are round, moderately dense, have a controlled size distribution, are easy to filter and free flowing. The key rate processes that control the kinetics and granule properties are breakage of drops and low density agglomerates and immersion nucleation (*Stage I*) and agglomerate densification through collisions with layered growth (*Stages II* and *III*).

The kinetics of agglomeration are intrinsically linked to the agglomerate densification kinetics (Fig. 6 and Fig. 7). Agglomeration is complete once all primary particles are captured. Tash et al. [33] quantified immersion nucleation kinetics showing the nucleation time could be controlled by either the rate of capilliary driven immersion of particles into the dispersed phase or the collision rate of particles with the drops. For the system under study in this paper, the time scales for immersion and collision controlled nucleation are of order 10^{-3} s and 300 s respectively, indicating nucleation kinetics are controlled by particle-drop collision. However, agglomerate density continues to increase, and free fines decrease for up to 160 min (~10^4s). Immersion nucleation as described by Tash et al. only dominates in the first few minutes of agglomeration (*Stage I*), and another mechanism must control this second stage of agglomeration (*Stage II*).

We propose the second, slower stage of agglomeration is controlled by agglomerate densification (consolidation) due to collisions between agglomerates and the impeller or wall of the vessel. Immersion nucleation in *Stage I* creates a shell that locks in a structure which resists further densification driven by capilliary forces. Rearrangement of particles which is required by the spherical geometry for further particle layer penetration is not possible without external impact. This hypothesis is supported by agglomerate size measurements which show drop/agglomerate breakage only occurring in *Stage I* of agglomeration, after which the agglomerates are too strong to break. This is analogous to granule consolidation observed during wet granulation. Iveson et al. [39] and Hounslow et al. [40] both proposed similar models for granulation where granule porosity (packing fraction) decreased via a first order process towards a critical packing fraction ϕ_{cp}. This consolidation process releases liquid at the agglomerate surface which captures additional primary particles.

Consider an agglomerate of size v consisting of a liquid volume v_L and solid volume v_S. During consolidation and layering, $v_L$does not change but v_S and v will increase. We write the following expressions for the agglomerate porosity (packing fraction) ϕ and dry density ρ_{agg}:

$$v(t) = v_S(t) + v_L \tag{4}$$

$$\phi(t) = \frac{v_L}{v_L + v_S(t)} \tag{5}$$

$$\rho_{agg}(t) = \big(1 - \phi(t)\big)\rho_t \tag{6}$$

where the subscripts L and S represent the dispersed liquid and primary particles respectively. We assume a first order decay of porosity towards the minimum porosity (critical packing fraction) ϕ_{cp}:

$$\frac{d\phi}{dt} = -K_c\big(\phi - \phi_{cp}\big) \tag{7}$$

where K_c is the consolidation rate constant (min^{-1}). Integrating this expression gives the exponential decay of ϕ with time:

$$\frac{(\phi(t) - \phi_{cp})}{(\phi_0 - \phi_{cp})} = exp(-K_c(t - t_0)) \tag{8}$$

where the subscript *0* denotes the start of the impact controlled consolidation (*Stage II*). Given $\phi(t)$ from Eq. (8), $\rho_{agg}(t)$, $v_S(t)$ and $v(t)$ can be calculated from Eqs. (4-6).

Similar to wet granule consolidation, we expect K_c to be a function of the amount of deformation in a single impact given in terms of the Stokes Deformation Number [39]:

$$K_c = f\big(St_{def}\big) \tag{9}$$

where

$$St_{def} = \frac{\rho_{agg} U_c^2}{2\sigma_Y} \tag{10}$$

and U_c is the characteristic collision velocity in the system and σ_Y is the plastic yield stress of the wet agglomerate. For a stirred tank agglomerator, impeller tip speed can be used as the characteristic collision velocity. Thus:

$$St_{def} = \frac{\rho_{agg} (\omega r)^2}{2\sigma_Y} \tag{11}$$

where ω is the angular velocity (rad.s^{-1}) and r is the impeller radius (m). We expect the yield stress to increase as agglomerate packing fraction decreases. If the strength follows a Rumpf style model [39], then:

$$\sigma_Y \propto \frac{1-\phi}{\phi} \tag{12}$$

The optimum *TBSR* should be above the critical value corresponding to a completely saturated agglomerate at its minimum porosity [34]:

$$TBSR > TBSR_{crit} = \frac{\phi_{cp}}{1-\phi_{cp}} \tag{13}$$

At $TBSR_{crit}$, it will take an infinite time for all primary particles to be included in the agglomerates. At $TBSR > TBSR_{crit}$, the porosity at which agglomeration is complete is:

$$TBSR = \frac{\phi_{agg}}{1-\phi_{agg}} \tag{14}$$

$$\phi_{agg} = \frac{TBSR}{1+TBSR} \tag{14a}$$

Rearranging Eq. (8) gives:

$$t_{agg} - t_0 = -\frac{1}{K_c} ln\left[\frac{\phi_{agg}-\phi_{cp}}{\phi_0-\phi_{cp}}\right] \tag{15}$$

Comparison with paracetamol-heptane-water system

This model gives a good qualitative and quantitative description of the case study system studied in this paper. The stable operating range for *TBSR* corresponds to *Regions B* and *C* in Fig. 3 (0.72 to 1.7), corresponding to a porosity range from 0.42 to 0.63. At *TBSR < 0.72*, agglomerate is not complete, while at *TBSR > 1.7* agglomerates are too weak to survive filtration.

Fig. 12 replots the porosity data corresponding to Fig. 7 within *Stage II* (>30 min). A best fit line for Eq. (12) is shown on Fig. 12a. The data is a good fit to the first order consolidation model (Eq. (12)) with $K_c = 0.030\ min^{-1}$ and $\phi_{cp} = 0.42$.

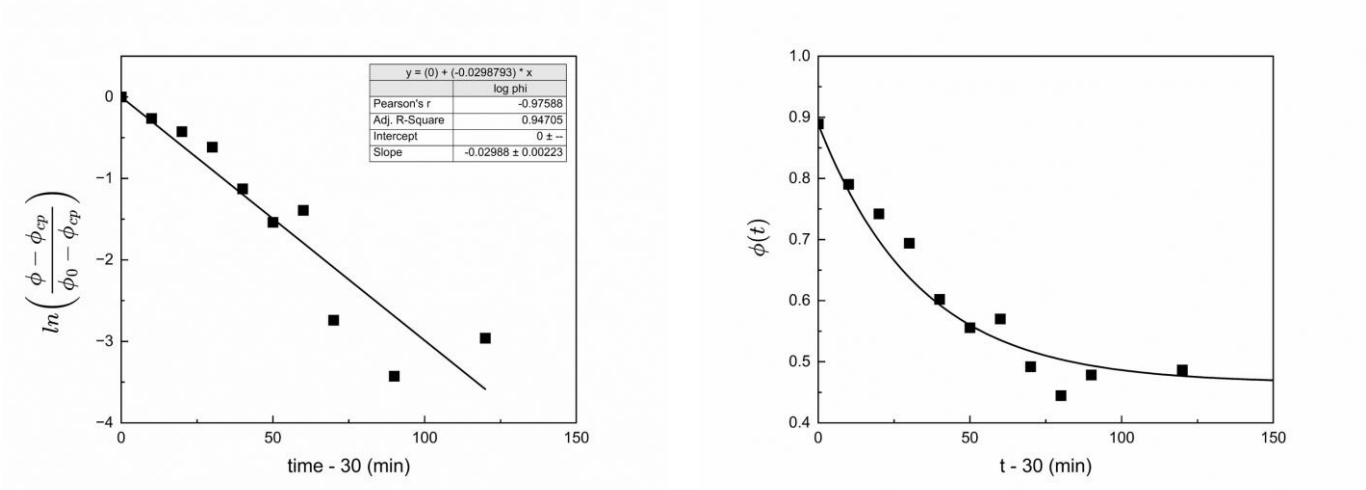

Fig. 12. Porosity change with time during agglomeration *Stage II*: Comparison of data with Eq. (8) (*TBSR* = 0.75, impeller speed = 500 rpm, Solids loading = 5 %)

Given agglomeration is fast, we expect t_{paste} to be similar to t_{agg}. The relationship between t_{paste} and $TBSR$ is therefore what we would expect from Eqs. (14) and (15). Fig. 13 shows a prediction of t_{paste} given $TBSR_{crit} = 0.72$, which matches the data remarkably well. The value of ϕ_{cp} is consistent with that measured directly for the agglomerate product at complete agglomeration in *Region C*, 0.41 ± 0.15 (Fig. 11b).

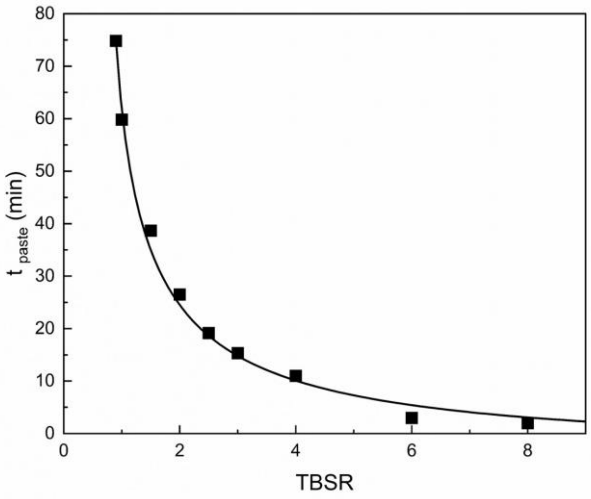

Fig. 13. Comparison of t_{paste} as a function of *TBSR* with that predicted by the model (impeller speed = 500 rpm, Solids loading = 5 %)

The model also predicts the effect of changing impeller speed. Increasing impeller speed will increase K_c (Eqs. (9) and (11)) resulting in shorter agglomeration times (Fig. 9a). Note that ϕ_{cp} also decreases with increasing impeller speed (Fig. 9b). As expected, increased impeller speed leads to more drop breakage in *Stage I* and therefore smaller agglomerates (Fig. 9c and Fig. 9d). Increasing impeller speed gives smaller, denser granules with shorter agglomeration times and a smaller value for $TBSR_{crit}$.

Implications for design space, kinetics and agglomerate attributes

One limit on design space is given by the maximum acceptable agglomeration time $t_{agg,max}$, then combining Eqs. (14a) and (15) for $t_{agg} = t_{agg,max}$:

$$t_{agg,max} - t_0 = -\frac{1}{K_c} ln\left[\frac{TBSR_{min} - TBSR_{cp}}{1 + TBSR_{min}}\right] \tag{16}$$

As *TBSR* increases, the strength of the agglomerates will decrease (Eq. (12)). Another limit on the design space will be the minimum strength required for agglomerates to survive filtration and drying, σ_{min}. Comparing Eqs. (12) and (14):

$$\sigma_Y \propto \frac{1}{TBSR} \tag{17}$$

and

$$\frac{TBSR_{max}}{TBSR_{crit}} = \frac{\sigma_{crit}}{\sigma_{min}} \tag{18}$$

These relationships are shown in Fig. 14 in nondimensional form. While agglomerate size is set by drop breakage in stage I, the agglomeration time, feasible range of *TBSR,* agglomerate density and strength are all primarily determined agglomerate consolidation. Fig. 14 is general for any agglomeration system. The key parameters required for the design space calculations are K_c and ϕ_{cp}. Currently, no standard methods are available to measure these parameters, but the methodology developed in this paper gives a good starting point for such a development.

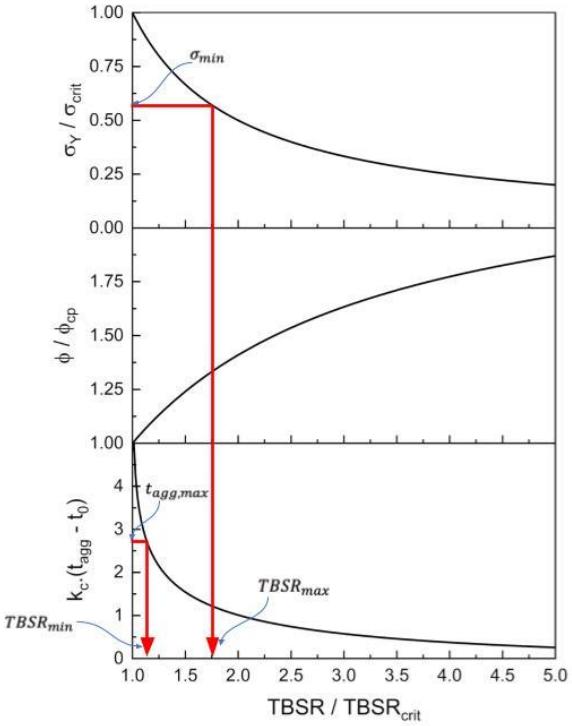

Fig. 14. Non-dimensional relationship between *TBSR* and agglomeration time, agglomerate strength and porosity. Design space of *TBSR* bounded by the maximum allowable agglomeration time and the minimum allowable agglomeration strength.

Note that many pharmaceutical systems have partial solubility between the continuous solvent/antisolvent phase and the binding liquid. In this case, *BSR* > *TBSR*. However, *TBSR* can be calculated relatively easily if the phase diagram is known [34].

These results show impeller speed is a sensitive and important parameter to evaluate when developing the design space for spherical agglomeration, being important to determining both agglomerate size and density. In some cases, the coupling between small and dense agglomerates may be undesirable, e.g. if dense agglomerates slow down the dissolution profile of the tableted product. It is possible to decouple size and density if drop size is controlled at the desired agglomerate size when the binder liquid is added to the vessel, taking advantage of the immersion nucleation mechanism [20, 33]. The effect of solids loading on agglomeration kinetics and properties is more complex. While increasing solids loading gives a smaller and narrower agglomerate size distribution, with denser agglomerates, the major impact is to dramatically increase the required time for complete agglomeration. These results suggest solids loading above 5 % are not practical. Keeping solids loading constant during scale up is recommended.

5. Conclusions

The paracetamol-heptane-water system has been used to study the immersion nucleation mechanism with the aim of further developing our mechanistic understanding of the spherical agglomeration process. This includes the formation of agglomerate nuclei and their evolution process to dense, spherical agglomerates. Here, a critical range of a *TBSR* of 0.72 – 0.8 was identified where moderately dense, round agglomerates with controlled size were formed. Four other distinct regions of operation were observed. These regions were identified by significant changes in the agglomerate properties and are also characterised by whether or not a paste forms and the time required for the onset of paste formation.

Agitation rate had a significant effect on the properties of the agglomerates. An increase in impeller speed resulted in a decrease in agglomerate size and porosity and also reduced the agglomeration time. The critical *TBSR* range was found to be independent of solid loading. However, there was an effect of solid loading on agglomerate properties; higher loadings produced smaller agglomerates with lower porosities. Increased solids loading also caused a large increase in the agglomeration time.

The time scale for complete agglomeration is significantly longer than that predicted by immersion nucleation kinetics alone. Rather, agglomeration consolidation by impact largely determines the required agglomeration time. A first

order consolidation model borrowed from granulation literature gives a very good fit to the agglomerate porosity and successfully predicts the reduction in time to paste and agglomerate strength at *TBSR* increases, leading to preliminary recommendations for a process design and scale up methodology.

Acknowledgements

This work was supported by the EPSRC Future Continuous Manufacturing and Advanced Crystallisation Research Hub (Grant Ref: EP/P006965/1) and CMAC Tier 1 companies: AstraZeneca, Pfizer, Takeda and Eli Lilly. The authors would like to thank Shekar Viswanath (Eli Lilly), Masashi Furuta (Takeda) and Naila Mugheribi (Pfizer) for useful discussions, and Jediah Capindale for producing Figs. 12 to 14.

References

[1] M. Leane, K. Pitt, G.K. Reynolds, N. Dawson, I. Ziegler, A. Szepes, A.M. Crean, R. Dall Agnol, M.C.S.W. Group, Manufacturing classification system in the real world: factors influencing manufacturing process choices for filed commercial oral solid dosage formulations, case studies from industry and considerations for continuous processing, Pharm. Dev. Technol. 23 (2018) 964-977.

[2] N. Variankaval, A.S. Cote, M.F.J.A.J. Doherty, From form to function: Crystallization of active pharmaceutical ingredients, AIChE J. 54 (2008) 1682-1688.

[3] G. Perini, F. Salvatori, D.R. Ochsenbein, M. Mazzotti, T. Vetter, Filterability prediction of needle-like crystals based on particle size and shape distribution data, Sep. Purif. Technol. 211 (2019) 768-781.

[4] O.S. Agimelen, A.J. Mulholland, J. Sefcik, Modelling of artefacts in estimations of particle size of needle-like particles from laser diffraction measurements, Chem. Eng. Sci. 158 (2017) 445-452.

[5] L.E. Hatcher, W. Li, P. Payne, B. Benyahia, C.D. Rielly, C.C. Wilson, Tuning morphology in active pharmaceutical ingredients: controlling the crystal habit of lovastatin through solvent choice and non-size-matched polymer additives, Cryst. Growth Des. 20 (2020) 5854-5862.

[6] S. Kim, B. Lotz, M. Lindrud, K. Girard, T. Moore, K. Nagarajan, M. Alvarez, T. Lee, F. Nikfar, M. Davidovich, Control of the particle properties of a drug substance by crystallization engineering and the effect on drug product formulation, Org. Process Res. Dev. 9 (2005) 894-901.

[7] B. Ahmed, C.J. Brown, T. McGlone, D.L. Bowering, J. Sefcik, A.J. Florence, Engineering of acetaminophen particle attributes using a wet milling crystallisation platform, Int. J. Pharm. 554 (2019) 201-211.

[8] W. Meng, E. Sirota, H. Feng, J.P. McMullen, L. Codan, A.S. Cote, Effective Control of Crystal Size via an Integrated Crystallization, Wet Milling, and Annealing Recirculation System, Org. Process Resd. Dev. 24(11) (2020) 2639-2650.

[9] C.J. Brown, T. McGlone, S. Yerdelen, V. Srirambhatla, F. Mabbott, R. Gurung, M.L. Briuglia, B. Ahmed, H. Polyzois, J. McGinty, F. Perciballi, D. Fysikopoulos, P. MacFhionnghaile, H. Siddique, V. Raval, Y.S. Harrington, A.D. Vassileiou, M. Robertson, E. Prasad, A. Johnston, B. Johnston, A. Norden, J.S. Srai, G. Halbert, J.H. ter Horst, C.J. Price, C.D. Reilly,

J. Sefcik, A.J. Florence, Engineering, Enabling precision manufacturing of active pharmaceutical ingredients: workflow for seeded cooling continuous crystallisations, Mol. Syst. Des. Eng. 3 (2018) 518-549.

[10] L. Schenck, D. Erdemir, L.S. Gorka, J.M. Merritt, I. Marziano, R. Ho, M. Lee, J. Bullard, M. Boukerche, S. Ferguson, A.J. Florence, S.A. Khan, C.C. Sun, Recent Advances in Co-Processed APIs and Proposals for Enabling Commercialization of These Transformative Technologies, Mol. Pharm. 17(7) (2020) 2232-2244.

[11] K. Pitt, R. Peña, J.D. Tew, K. Pal, R. Smith, Z.K. Nagy, J.D.J.P.t. Litster, Particle design via spherical agglomeration: A critical review of controlling parameters, rate processes and modelling, Powder Technol. 326 (2018) 327-343.

[12] A. Sirianni, C. Capes, J. Puddington, Recent experience with the spherical agglomeration process, Can J. Chem. Eng. 47 (1969) 166-170.

[13] J. Sutherland, The agglomeration of aqueous suspensions of graphite, Can. J. Chem. Eng. 40 (1962) 268-272.

[14] Y. Kawashima, C. Capes, Further studies of the kinetics of spherical agglomeration in a stirred vessel, Powder Technol. 13 (1976) 279-288.

[15] L. Schenck, A. Koynov, A. Cote, Particle engineering at the drug substance, drug product interface: a comprehensive platform approach to enabling continuous drug substance to drug product processing with differentiated material properties, Drug Dev. Ind. Pharm. 45 (2019) 521-531.

[16] Y. Kawashima, M. Imai, H. Takeuchi, H. Yamamoto, K. Kamiya, T. Hino, Improved flowability and compactibility of spherically agglomerated crystals of ascorbic acid for direct tableting designed by spherical crystallization process, Powder Technol. 130 (2003) 283-289.

[17] C.L. Viswanathan, S.K. Kulkarni, D.R. Kolwankar, Spherical agglomeration of mefenamic acid and nabumetone to improve micromeritics and solubility: A technical note, AAPS PharmSciTech, 7 (2006) E122-E125.

[18] A. Nokhodchi, M. Maghsoodi, D. Hassan-Zadeh, M. Barzegar-Jalali, Preparation of agglomerated crystals for improving flowability and compactibility of poorly flowable and compactible drugs and excipients, Powder Technol. 175 (2007) 73-81.

[19] J. Thati, Å.C. Rasmuson, Particle engineering of benzoic acid by spherical agglomeration, Eur. J. Pharm. Sci. 45 (2012) 657-667.

[20] P.M. Orlewski, B. Ahn, M. Mazzotti, Tuning the particle sizes in spherical agglomeration, Cryst. Growth Des. 18 (2018) 6257-6265.

[21] K. Kedia, S. Wairkar, Improved micromeritics, packing properties and compressibility of high dose drug, Cycloserine, by spherical crystallization, Powder Technol. 344 (2019) 665-672.

[22] A. Blandin, D. Mangin, A. Rivoire, J.P. Klein, J.M. Bossoutrot, Agglomeration in suspension of salicylic acid fine particles: influence of some process parameters on kinetics and agglomerate final size, Powder Technol. 130 (2003) 316-323.

[23] R. Kuboi, A. Nienow, R. Conti, Mechanical attrition of crystals in stirred vessels, Ind. Cryst. 84 (1984) 211-216.

[24] L. Madec, L. Falk, E. Plasari, Modelling of the agglomeration in suspension process with multidimensional kernels, Powder Technol. 130 (2003) 147-153.

[25] R. David, A.-M. Paulaime, F. Espitalier, L. Rouleau, Modelling of multiple-mechanism agglomeration in a crystallization process, Powder Technol. 130 (2003) 338-344.

[26] A.F. Blandin, D. Mangin, C. Subero-Couroyer, A. Rivoire, J.P. Klein, J.M. Bossoutrot, Modelling of agglomeration in suspension: Application to salicylic acid microparticles, Powder Technol. 156 (2005) 19-33.

[27] R. Peña, C.L. Burcham, D.J. Jarmer, D. Ramkrishna, Z.K. Nagy, Modeling and optimization of spherical agglomeration in suspension through a coupled population balance model, Chem. Eng. Sci. 167 (2017) 66-77.

[28] B. Ahmed, O. Arjmandi-Tash, J.D. Litster, R.M. Smith, Mechanistic modelling of spherical agglomeration processes, Powder Technol. 417 (2023) 118254

[29] R. Peña, D.J. Jarmer, C.L. Burcham, Z.K. Nagy, Further understanding of agglomeration mechanisms in spherical crystallization systems: benzoic acid case study, Cryst. Growth Des. 19 (2019) 1668-1679.

[30] M. Chen, X. Liu, C. Yu, M. Yao, S. Xu, W. Tang, X. Song, W. Dong, G. Wang, J. Gong, Strategy of selecting solvent systems for spherical agglomeration by the Lifshitz-van der Waals acid-base approach, Chem. Eng. Sci. 220 (2020) 115613.

[31] X. Cheng, F. Li, L. Luo, Z. Ding, L. Zeng, Y. Mao, X. Huang, H. Hao, On the selection of wetting liquid for spherical agglomeration of cefotaxime sodium, Powder Technol. 363 (2020) 593-601.

[32] C. Subero-Couroyer, D. Mangin, A. Rivoire, A. Blandin, J. Klein, Agglomeration in suspension of salicylic acid fine particles: Analysis of the wetting period and effect of the binder injection mode on the final agglomerate size, Powder Technol. 161 (2006) 98-109.

[33] O. Arjmandi-Tash, J.D. Tew, K. Pitt, R. Smith, J.D. Litster, A new mathematical model for nucleation of spherical agglomerates by the immersion mechanism, Chem. Eng. Sci. X, 4 (2019) 100048.

[34] J.D. Tew, K. Pitt, R. Smith, J.D. Litster, True bridging liquid-solid ratio (TBSR): Redefining a critical process parameter in spherical agglomeration, Powder Technol. 430 (2023) 119010

[35] J. Thati, Å.C. Rasmuson, On the mechanisms of formation of spherical agglomerates, Eur. J. Pharm. Sci. 42 (2011) 365-379.

[36] J. Katta, C. Rasmuson, Spherical crystallization of benzoic acid, Int. J. Pharm. 348 (2008) 61–69.

[37] M. Maghsoodi, Effect of process variables on physicomechanical properties of the agglomerates obtained by spherical crystallization technique, Pharm. Dev. Technol. 16 (2011) 474–482.

[38] A.R. Paradkar, A.P. Pawar, J.K. Chordiya, V.B. Patil, A.R. Ketkar, Spherical crystallization of celecoxib, Drug Dev. Ind. Pharm. 28 (2002) 1213–20.

[39] S.M. Iveson. J.D Litster, K. Hapgood, B.J. Ennis, Nucleation, growth and breakage phenomena in agitated wet granulation processes: a review, Powder Technol. 117 (2001) 3-39.

[40] M.J. Hounslow, M. Oullion, G.K.Reynolds, Kinetic models for granule nucleation by the immersion mechanism, Powder Technol. 189 (2009) 177-189.